LASER APPLICATIONS AND OTHER TOPICS IN QUANTUM ELECTRONICS https://doi.org/10.1070/QEL16613

Reflective mode X-ray microscopy of inclined objects

I.A. Artyukov, A.S. Busarov, A.V. Vinogradov, N.L. Popov

Abstract. **We propose an optical configuration of a reflective mode X-ray microscope which operates by the reflection of radiation incident on an object at grazing incidence. Primary emphasis is placed on the image recording with minimal aberrations. Numerical simulations are used to estimate the spatial resolution and the field of view, and a comparison is made with the results of investigation of surface-modified objects with a reflective mode X-ray laser microscope operating at a wavelength of 14.9 nm.**

Keywords: *X-ray microscopy, X-ray lasers, coherent optics, inclined object, Fresnel integral.*

1. Introduction

At present there is a demand for nanoscale surface investigations of various materials and processes. The cases in point are ablation, phase transitions, self-organisation, physico-chemical transformations, etc. [1, 2]. Since investigations are made of surfaces and the films on them, it would be natural to obtain their images with a microscope using the radiation reflected from the surface of a sample. Required in this case is the wavelength that can provide the corresponding resolution. On the one hand, the shorter the wavelength, the higher the resolution obtainable. One the other hand, of importance in some problems is the depth of radiation penetration in the material. In particular, it is undesirable that the probing radiation penetrates to a depth greater than the investigated layer thickness [1], which may be much thinner than the skin layer in the IR and visible wavelength ranges. Finally, with decreasing wavelength the sources and optics become less accessible and more expensive. In view of these factors, in many problems of nanophysics and nanotechnology the observations are carried out employing radiation with a photon energy of 0.1–10 keV. However, at these wavelengths a significant fraction of radiation is reflected only at small ($\leqslant 10°$) grazing angles. Therefore, this brings up the idea of making an X-ray microscope operating by the reflection of radiation incident on an object at grazing incidence. In this case, preference is shown to laser or other coherent radiation sources [1, 2] to illuminate the object. A possible optical scheme of this type of microscope is considered in our work. Among its topical applications is the diagnostics of submicron electron beams of modern accelerators [3].

I.A. Artyukov, A.S. Busarov, A.V. Vinogradov, N.L. Popov P.N. Lebedev Physical Institute, Russian Academy of Sciences, Leninsky prosp. 53, 119991 Moscow, Russia;
e-mail: albusarov@mail.ru, vinograd@sci.lebedev.ru

Received 28 January 2018; revision received 26 April 2018
Kvantovaya Elektronika **48** (7) 662–666 (2018)
Translated by E.N. Ragozin

2. Preliminary analysis, two-dimensional case

The generalised schematic of the proposed microscope is presented in Fig. 1. The radiation with a wave vector $\boldsymbol{k}$ is reflected from the surface of an inclined sample (*1*) and passes through a lens (*2*). In this case, in the geometrical optics approximation the lens forms an intermediate image in the plane optically conjugate to the object plane. To state it in different terms, the object and the image lie in the ray sAx', which passes through the lens. As shown by Artyukov et al. [4], in paraxial optics this remains approximately valid for coherent imaging as well.

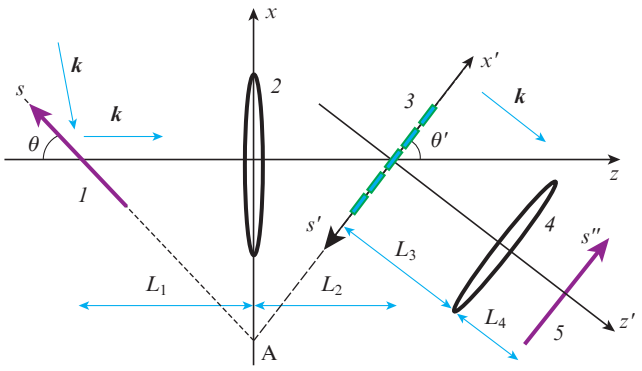

Figure 1. Optical schematic of the microscope (two-dimensional case): (*1*) object; (*2*, *4*) lenses; (*3*) diffraction grating (phase screen); (*5*) image (detector). The image and diffraction grating planes are optically conjugate relative to lens *2*, and the grating and image planes are optically conjugate relative to lens *4*.

When a detector is placed in the image plane, the grazing angle θ' relative to the detector may be written as

$$\tan\theta' = \frac{1}{M_0}\tan\theta, \tag{1}$$

where $M_0 = L_2/L_1$ is the magnification for a vertically positioned object. The magnification $M(\theta)$ of an inclined object is defined by the formula

$$M^2(\theta) = M_0^2\sin^2\theta + M_0^4\cos^2\theta, \tag{2}$$

which, as shown in Ref. [5], may be derived by transformation of the amplitude of coherent beam field. Evidently, for large $M(\theta)$ values

$$M_0 \approx \sqrt{\frac{M(\theta)}{\cos\theta}}, \tag{3}$$

i.e. at least $M_0 > 1$. Hence it follows, in view of formula (1), that $\theta' < \theta$, i.e. the image plane is located at a smaller angle than the sample. This image plane position is extremely undesirable due to the total external reflection of radiation not only from the sample, but also from the detector. It can be obviated by placing a diffraction grating (*3*) in plane s' to direct the beam in the direction perpendicular to the grating (see Fig. 1). Next lens (*4*)transfers the intermediate image onto a detector (*5*) at normal incidence.

The intermediate image, its magnification and position are defined by the relations [5]

$$I(s') = \frac{1}{M_0} I_0\left[\frac{s'}{M(\theta)}\right], \tag{4}$$

$$M(\theta) = M_0(\sin\theta)/(\sin\theta'), \tag{5}$$

$$\frac{1}{L_1} + \frac{1}{L_2} = \frac{1}{f_1}, \quad \tan\theta' = \frac{1}{M_0}\tan\theta, \quad M_0 = \frac{L_2}{L_1}, \tag{6}$$

where f_1 is the focal length of lens 2; $I(s')$ and $I_0(s)$ are the intensities of the intermediate image and the object.*

Therefore, the proposed microscope scheme consists of two parts separated by a diffraction grating. The wavelength choice and the optical parameters of either part are defined by the specific problem and available optical elements. The first part of the scheme consisting of an object (*1*), a lens (*2*), and a grating (*3*) provides rotation of the image plane to a more convenient form for further magnification and recording. In this case, the magnitude of $M(\theta)$ in this part of the optical scheme is of no fundamental importance. After the grating (*3*) the radiation passes through a lens (*4*) and is normally incident on the detector (*5*), which is located in the plane conjugate to the grating plane relative to the lens (*4*). This is the second part of the optical scheme. It, in fact, forms the magnified image.

3. Three-dimensional geometry

Let us consider the three-dimensional case. The intermediate image intensity distribution (Fig. 2) is defined by the expression [5]

$$I(s', y') = \frac{1}{M_0^2} I_0\left[\frac{s'}{M(\theta)}, \frac{y'}{M_0}\right], \tag{7}$$

where $M(\theta)$, M_0 and the relations between θ and θ' are defined, like in the two-dimensional geometry, by formulas (5) and (6).

Therefore, the magnification along the s' axis is equal to $M(\theta)$ and along the y' axis is equal to M_0. We also give the formula for the image magnification along the direction specified by an angle ψ in the object plane:

$$M(\theta, \psi) = M_0\sqrt{1 + (M_0^2 - 1)\cos^2\theta\cos^2\psi}\,. \tag{8}$$

Expressions (7) and (8) generalise to the three-dimensional case formulas (4) and (5) for the intermediate image.

*Expressions (4) and (5) are approximate, more rigorous relationships can be found in Ref. [5].

4. Numerical simulations

To estimate the spatial resolution, we performed numerical simulations of the configuration given in Fig. 2. To this end, a test field distribution was specified in the object plane (*1*). Based on this distribution, we proceeded along the optical axis by calculating the field sequentially in the planes (*2–4*) of the optical elements subject to the transformation by these elements. After that, the resultant field was calculated in the detector plane (*5*).

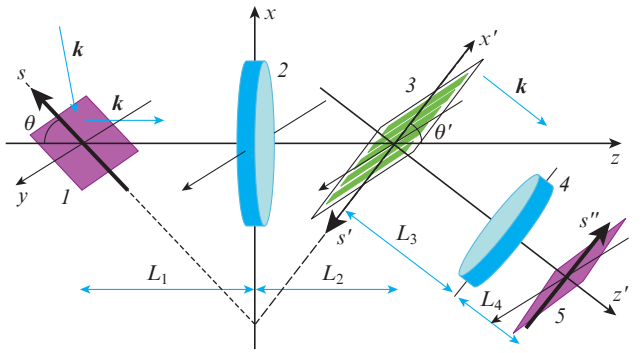

Figure 2. Optical schematic of the microscope (three-dimensional geometry):
(*1*) object; (*2*,*4*) lenses; (*3*) diffraction grating (phase screen); (*5*) image (detector). The image and diffraction grating planes are optically conjugate relative to lens *2*, and the grating and image planes are optically conjugate relative to lens *4*.

To calculate the field at the left surface of lens *2* produced by the test distribution in the object plane (*1*), we used an analogue of the Fresnel integral in the case of a tilted object, a tilted object integral (TOI) [6], in the three-dimensional case:

$$u(x, y, z) = \frac{k(x + z\tan\theta)}{2\pi\mathrm{i}} \int_{-\infty}^{\infty} \mathrm{d}y' \int_{-\infty}^{z} \frac{u_0(y', z')\,\mathrm{d}z'}{(z - z')^2} \times \exp\left[\mathrm{i}k\frac{(y - y')^2 + (x + z'\tan\theta)^2}{2(z - z')}\right], \; x > -z\cos\theta. \tag{9}$$

The field at the right side of lens *2* was obtained as the product of the field $u(x, y, z)$ and the factor

$$T(x, y) = \exp[-\mathrm{i}k(x^2 + y^2)/(2f_1)], \tag{10}$$

which describes the transformation effected by the lens [f_1 is the focal distance of lens (*2*)].

Next, to calculate the field in the intermediate image plane (*3*), advantage was taken of the ordinary Fresnel integral. Without changing the slowly varying field amplitude u, the diffraction grating (*3*) turns the direction of wave propagation by an angle $\pi/2 - \theta'$, i.e. the radiation propagates perpendicular to the grating after passing through it.

Subsequently the field at lens *4* was once again calculated with the ordinary Fresnel integral. Lens *4* acts in the same way as lens *2*, in accordance with formula (10), except that it has a focal distance f_2. After that the field at the detector was determined, also using the Fresnel integral. The inclined-object field (9), like the Fresnel integral, was calculated by the fast Fourier transform algorithm [7].

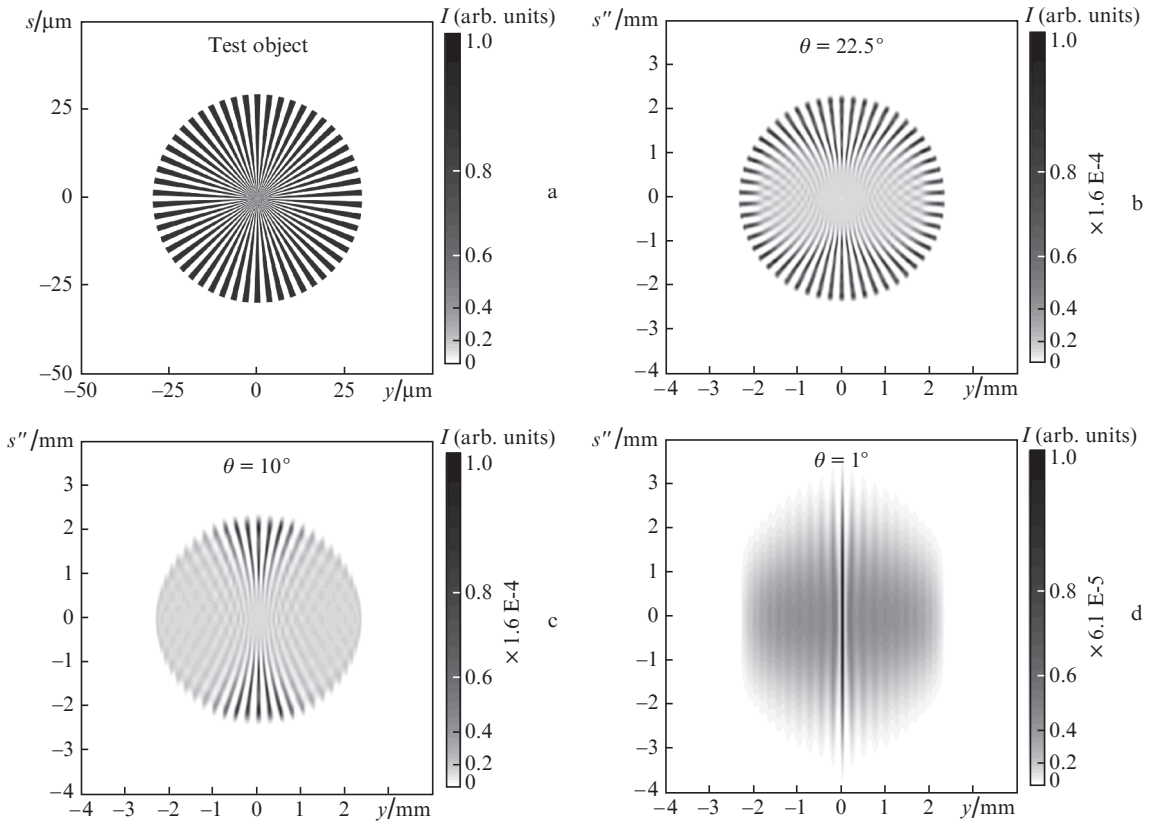

Figure 3. (a) Test object in the form of a star and (b, c, d) results of numerical simulation of the the object's image for different angles of grazing beam incidence: θ = (b) 22.5, (c) 10 and (d) 1°.

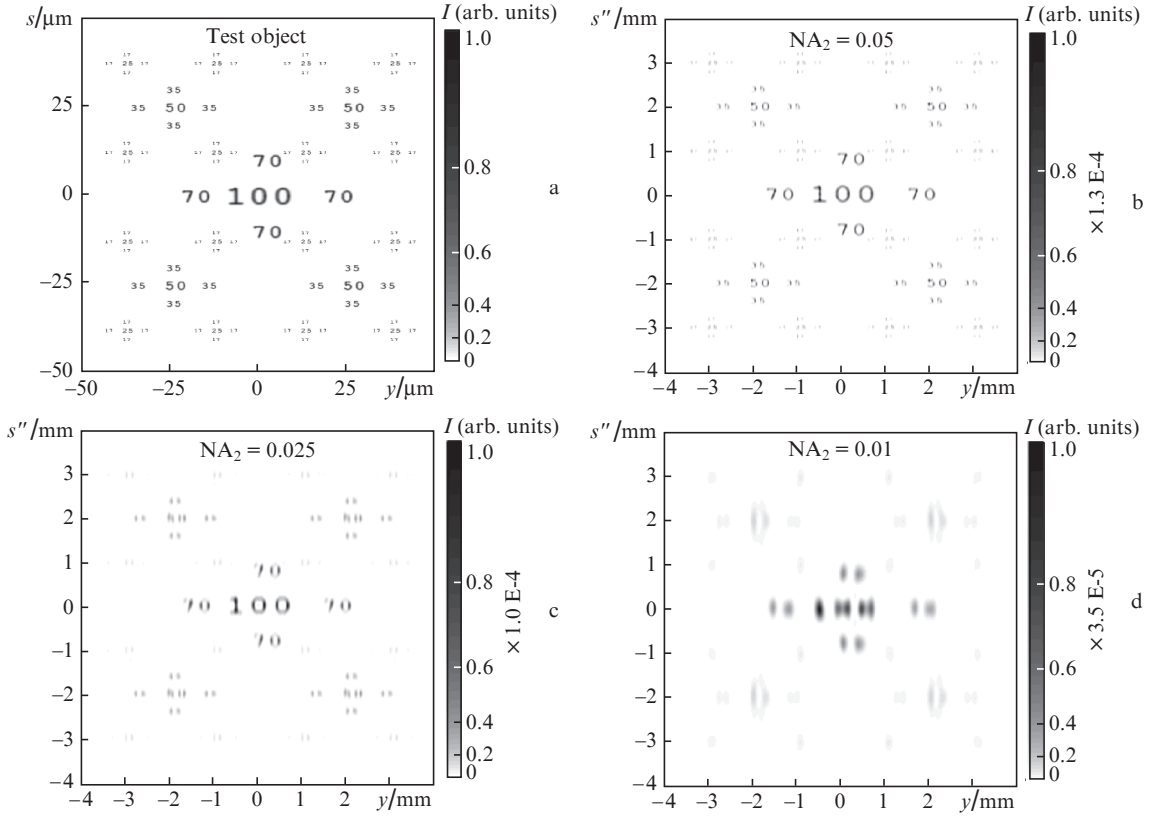

Figure 4. (a) Test object in the form of numerals of different size located at different distances from the optical axis and (b, c, d) results of the numerical simulation of object images for second lens apertures NA_2 = (b) 0.05, (c) 0.025, and (d) 0.01.

Figure 3 shows the results of simulations which permit estimating the influence of angle θ on the resolution of the optical system schematised in Fig. 2. The simulations were performed for the following parameters: wavelength $\lambda = 13.9$ nm, numerical apertures of the lenses (*2*) and (*4*) $NA_1 = NA_2 = 0.025$, $f_1 = f_2 = 1$ cm, $L_1 = L_2 = 2f_1$, $L_3 = 1.0127$ cm, $L_4 = 80$ cm. The object of size 100×100 μm is inclined at an angle of 22.5° to the optical axis. For the sake of verification we performed the simulation of the image of the vertical object. The resultant field distribution is little different from the initial field in the object plane plotted in Fig. 3a.

Now let us consider the effect of the aperture of the second lens (Fig. 4). The simulation was performed for the following parameters: $\lambda = 13.9$ nm, $\theta = 22.5°$, $NA_1 = 0.025$, $f_1 = f_2 = 1$ cm, $L_1 = L_2 = 2f_1$, $L_3 = 1.0127$ cm, $L_4 = 80$ cm. In this case, the aperture NA_2 was equal 0.05, 0.025, and 0.01 (object dimensions: 00×100 μm). With reference to the drawing, lowering the aperture NA_2, as would be expected, results in a blurring of the image.

It is of interest to compare the action of our proposed scheme (Fig. 2) with the action of the optical scheme described in Ref. [1] (Fig. 5). The efficiencies of both schemes may be compared using the simulation results presented in Fig. 6.

The image of a test object (Fig. 6a) was calculated for our scheme (Fig. 2) for $\lambda = 13.9$ nm, $NA_1 = NA_2 = 0.025$, $f_1 = f_2 = 1$ cm, $L_1 = L_2 = 2f_1$, $L_3 = 1.0127$ cm, and $L_4 = 80$ cm. The angle of grazing beam incidence on the object $\theta = 22.5°$ (Fig. 6b) and 10° (Fig. 6c). Figure 6d shows the simulation results for the optical configuration schematised in Fig. 5, which were obtained for the following parameters: $\lambda = 13.9$ nm, $NA = 0.025$, $f = 1$ cm, $L = 80$ cm, $L_0 = 1.0127$ cm, and $\theta = 22.5°$. When comparing Figs 6b and 6d one can see that our proposed scheme shows a slight degradation of the image quality but provides a larger field of view.

We note the optical elements involved in our proposed scheme, the lenses and the diffraction grating for which numerical simulations were performed, were assumed to be perfect and were presented as phase screens. In the case of a real grating, its image is partly superimposed on the image, i. e. it is valid to say that the grating is illuminated with an intermediate image. The resultant image in the plane s'' will be only slightly distorted when the characteristic size of the features of the intermediate image exceeds the grating spacing d. When then the characteristic size δ of the smallest elements of the intermediate image pattern on the grating surface is much greater than the grating spac-

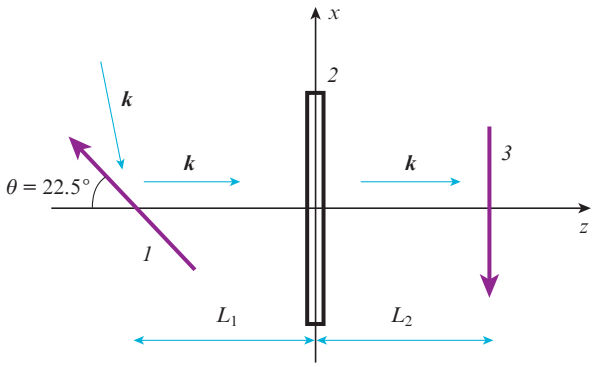

Figure 5. Simplified optical schematic of the experiment described in Ref. [1]:
(*1*) sample; (*2*) lens (Fresnel zone plate); (*3*) detector.

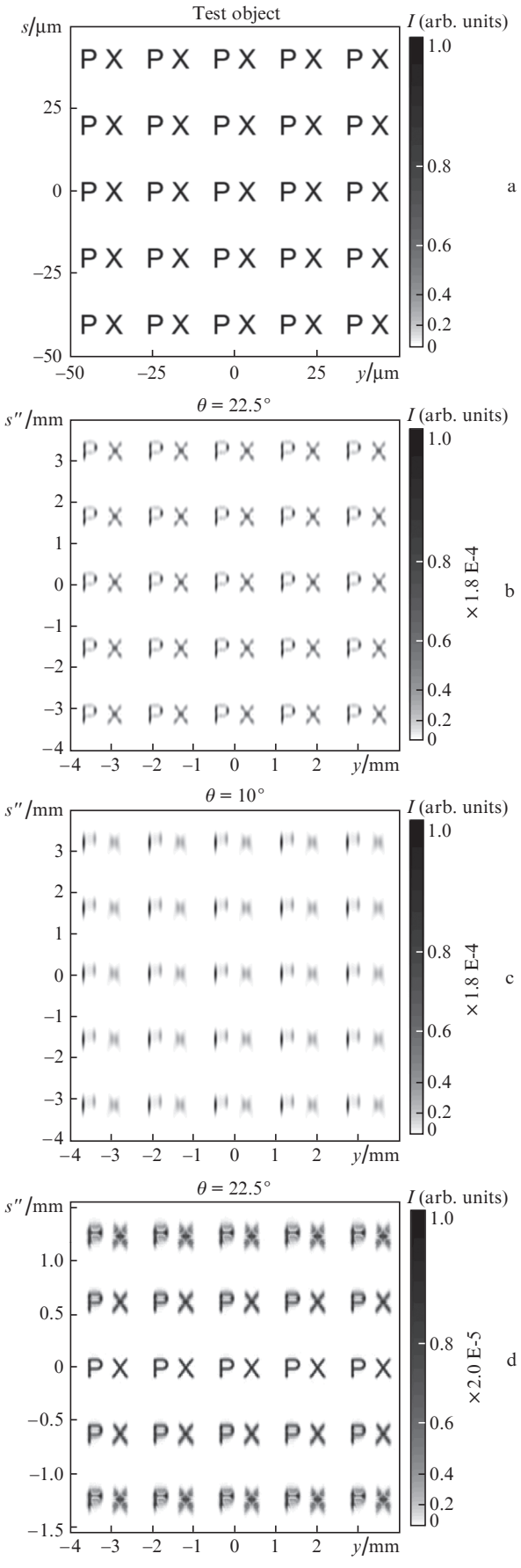

Figure 6. (a) Test object and (b, c, d) results of numerical simulations for the optical schemes depicted in Fig. 2 (b and c) and Fig. 5 (d).

ing d, i. e. $\delta \gg d$ [**], the resultant image distortion arising from the relief or structure of the grating is insignificant. However, when the image element is comparable in size to the grating spacing, significant distortions will emerge. Since the grating spacing

$$d = n\lambda/\cos\theta', \tag{11}$$

there appears an additional limitation on the size of the image element at the grating plane: $\delta \gg \lambda$.

5. Conclusions

This work proposes an optical configuration of a reflective mode X-ray microscope which operates by the reflection of radiation incident on an object at grazing incidence. In this case, one can avoid problems with low reflectivity of the samples under investigation at large angles of the incident radiation. The optical configuration comprises two focusing elements and a diffraction grating, which provides the normal incidence of radiation on the detector. Direct numerical simulations bear out the similarity between the image and the object down to grazing angles of $\sim 10°$.The proposed microscope possesses an appreciably larger field of view in comparison with the simplest configuration comprising a single optical element (a zone plate in the case of Ref. [1]). Model simulations and a comparison with experiment were performed for the $\lambda = 13.9$ nm wavelength of laboratory X-ray lasers. A further elaboration of the proposed optical configuration may involve a displacement of the diffraction grating from the intermediate image plane so as to improve the image quality at the detector. In this case, simulations can also be carried out using our developed programs.

The results of our work may be of interest in the nanometre surface investigation as well for the submicron diagnostics of electron beams from the transition radiation in the vacuum UV region.

Acknowledgements. This work was supported by the Programme of Scientific Investigations of the Presidium of the Russian Academy of Sciences 'Topical Problems of Photonics and Probing of Inhomogeneous Media and Materials' (PP RAS No. 7).

References

1. Baba M., Nishikino M., Hasegawa N., Tomita T., Minami Y., Takei R., Yamagiwa M., Kawachi T., Suemoto T. *Japan. J. Appl. Phys.*, **53**, 080302 (2014).
2. Laanait N., Callagon E.B.R., Zhang Z., Sturchio N.C., Lee S.S., Fenter P. *Science*, **349**, 6254 (2015).
3. Sukhikh L.G., Kube G., Bajt S., Lauth W., Popov Yu.A., Potylitsyn A.P. *Phys. Rev. ST Accel. Beams*, **17**, 112805 (2014).
4. Artyukov I.A., Busarov A.S., Popov N.L., Vinogradov A.V. *Proc. of the 13th Int. Conf. on X-Ray Lasers* (Paris, France: Springer Proceedings in Physics, 2014) Vol. 147, pp 19–27.
5. Artyukov I.A., Busarov A.S., Vinogradov A.V., Popov N.L. *Quantum Electron.*, **46** (9), 839 (2016) [*Kvantovaya Elektron.*, **46** (9), 839 (2016)].
6. Artyukov I.A., Feshchenko R.M., Popov N.L., Vinogradov A.V. *J. Opt.*, **16** (3), 035703 (2014).
7. Delen N., Hooker B. *J. Opt. Soc. Am. A*, **15**, 857 (1998).
8. Voronov D.L., Anderson E.H., Cambie R., Cabrini S., Dhuey S.D., Goray L.I., Gullikson E.M., Salmassi F., Warwick T., Yashchuk V.V., Padmore H.A. *Opt. Express*, **19** (7), 6320 (2011).

[**] This brings up a limitation on the resolving power of the microscope associated with the shortest attainable grating spacing. In particular, Voronov et al. [8] fabricated and tested gratings with a period of 100 nm.